International Journal of Mechanical, Industrial and Aerospace Sciences
ISSN: 2517-9950
Vol:9, No:4, 2015

CFD Study on the Effect of Primary Air on Combustion of Simulated MSW Process in the Fixed Bed

Rui Sun, Tamer M. Ismail, Xiaohan Ren, M. Abd El-Salam

***Abstract*—**Incineration of municipal solid waste (MSW) is one of the key scopes in the global clean energy strategy. A computational fluid dynamics (CFD) model was established in order to reveal these features of the combustion process in a fixed porous bed of MSW. Transporting equations and process rate equations of the waste bed were modeled and set up to describe the incineration process, according to the local thermal conditions and waste property characters. Gas phase turbulence was modeled using k-ε turbulent model and the particle phase was modeled using the kinetic theory of granular flow. The heterogeneous reaction rates were determined using Arrhenius eddy dissipation and the Arrhenius-diffusion reaction rates. The effects of primary air flow rate and temperature in the burning process of simulated MSW are investigated experimentally and numerically. The simulation results in bed are accordant with experimental data well. The model provides detailed information on burning processes in the fixed bed, which is otherwise very difficult to obtain by conventional experimental techniques.

***Keywords*—**Computational Fluid Dynamics (CFD) model, Waste Incineration, Municipal Solid Waste (MSW), Fixed Bed, Primary air.

I. Introduction

WASTE incineration power generation is one of the best waste disposal methods. Mechanical grate incinerator in new large-scale domestic waste incineration plants has been widely used. Relative to conventional coal-fired boilers, the physical and chemical reaction process waste incineration furnace is more complex [1].

Numerous theoretical studies on modeling MSW incineration have been published literature, based on many parameters. These simulations, helping in recognizing the behavior of gas and solid flow within the fixed bed [2], [3] and also the chemical process reactions [4], [5]. Yang et al. [6] for example, investigated the effects of fixed bed primary air proportion and fuel moisture content in the combustion process. They used biomasses and simulated MSW as fuels to investigate the variation of the moisture evaporation rate, volatile release, char combustion experimentally and numerically.

Yang et al. [7] performed experiments on fixed bed, investigating the effects of ignition time, burning rate, thickness of reaction area, temperature of flame fronts and gas species released at the top of the bed on devolatization rate and moisture content.

Ryu et al. [8] and Saastanainen et al. [9] investigated the propagation process of reaction fronts in fixed bed using wood as fuel, and also investigated air flow rate, moisture, particle size, density, and the effects of wood on flame reaction rate and the highest temperatures in fixed bed, and thus found out that the highest propagation speed can be observed depending on the relation between air and speed. But on the other hand, they didn't investigate the characteristic variations of fuel and temperature in fixed bed. Goh et al. [10], [11] also measured the temperature of MSW burning fuel at the top of the fixed bed and the gas component distribution. Zakaria et al. [12] investigated how to decrease the NOx production in MSW incinerator. Rönnbäck et al. [13] also investigated the effects of primary air and fuel characteristics on bed biomass ignition fronts, temperature and gas components of the fixed bed. Sharifi [14], Thunman et al. [15] carried out deliberate experiments and numerical researches on waste characteristics, bed temperature and gas components in middle- sized and large scale moving beds.

Discrete element method (DEM) and the continuum description model are the two different models applied to key out the gas-solid flow [16]. Discrete element method is the most popular model used, merely due to the increasing in the particle number the model becomes more expensive computationally because it requires high memory resources to overcome these calculations [17], [18]. On the other hand, the continuum model that based on kinetic theory of granular flow (KTGF) becomes a more general method employed in identifying the two phase model, particularly its use little CPU and less memory resources [19], [20].

Because above researches provide very few investigations for fuel and NO in the fixed bed, more deep and thorough researches are needed to investigate the effects of the combustion process on waste layers. A mathematical model of the fixed bed in the present work will be simulated using a new development code, namely COMMENT-Code (Combustion Mathematics and Energy Transport) to simulate the processes rate and combustion process within the bed, based on previous work [19], [20].

The present study provides a deliberate numerical and experimental investigation for the variation of temperature distribution, gas concentration, and mass in the fixed bed versus time during the combustion process, and this is done according to the variations of primary air, primary air temperature, and characteristics of simulated MSW, in order to understand the effects of primary air, primary air

Rui Sun and Xiaohan Ren are with School of Energy Science and Engineering, Harbin Institute of Technology, 92, West Dazhi Street, Harbin 150001, PR China (e-mail: sunsr@hit.edu.cn, sunsr@hit.edu.cn).

Tamer M. Ismail is with Department of Mechanical Engineering, Suez Canal University, Ismailia, Egypt (e-mail: temoil@aucegpt.edu tamer.ismail@eng.suez.edu.eg)

M. Abd El-Salam is with Department of Basic Science, Cairo University, Giza, Egypt (e-mail: mohamedelsheikh@cu.edu.eg).

temperature, and characteristics of simulated MSW on waste combustion process in the fixed-bed, which will provide references for engineering applications that can be useful for optimizing numerical models for MSW incineration and layered waste combustion.

II. Experimental Test Rig

A fixed-bed reactor was employed to burn simulated solid wastes. The reactor shown in Fig. 1 is a vertical cylindrical combustion chamber suspended from a weighing scale. The height of the chamber is 1.3 m with an inner diameter of 180 mm. The experimental combustor is axially symmetric and thermally insulated by a 50mm refractory wall. It consists of an interior tube surrounded by a thick layer of insulating material and an external casing. The grate is installed at the bottom of the chamber and consists of a perforated plate made from stainless steel, with approximately 95 holes of 7 mm diameter, representing 15% open area. Thermocouples were used to monitor the temperature of primary airflow, temperature inside the bed at different height levels (T1, T2 to T11). This system has been described in [21].

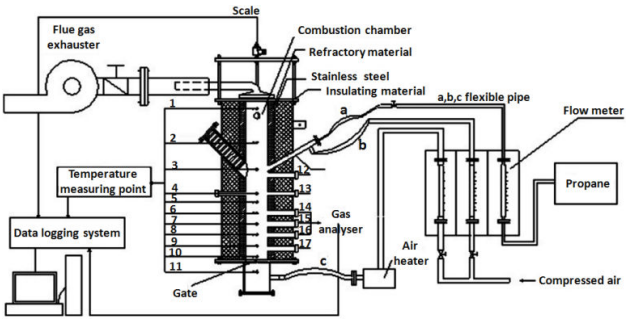

Fig. 1 Experimental one-dimensional fixed bed combustion test rig for simulated MSW

III. Mathematical Modeling of Fixed Bed

The mathematical model presented in the current work will be developed to simulate the processes rate and combustion process within the bed combustion. The model will be divided into two parts: firstly the process rate models and then the conservation (transport) equation model for gas and solid phases.

A. Process Rate Equations

1. Drying [22]

$$R_{evp} = A_s h_s (C_{w,s} - C_{w,g}) T_s < 100℃ \quad (1)$$

$$\text{or } R_{evp} = \frac{Q_{cr}}{H_{evp}} T_s = 100℃ \quad (2)$$

$$Q_{cr} = A\left(h_s'(T_g - T_s) + \epsilon\delta(T_\infty^4 - T_s^4)\right) \quad (3)$$

2. Devolatilization [23]

$$R_v = -\rho_{sb}\frac{dY_v}{dt} = \rho_{sb} Y_v A_v exp\left(\frac{E_v}{RT}\right) \quad (4)$$

$$A_v = 3.63 \times 10^4\ {}^1/_S\ , \frac{E_v}{R} = 9340\ K \quad (5)$$

3. Combustion of Volatiles [20]

$$R = min[R_{kin}, R_{mix}] \quad (6)$$

$$R_{mix} = C_{mix}\rho_g \times A \times B \quad (7)$$

$$A = 150\frac{D_g(1-\phi)^{2/3}}{d_p^2\phi} + 1.75\frac{V_g(1-\phi)^{1/3}}{d_p\phi} \quad (7a)$$

$$B = min\left\{\frac{C_{fuel}}{S_{fuel}}, \frac{C_{O_2}}{S_{O_2}}\right\} \quad (7b)$$

The following expressions give the rate for each species:

$$R_{CH_4} = 59.8\, T_g P^{0.3} exp\left(\frac{-12{,}200}{T_g}\right) C_{CH_4}^{0.5} \quad (8)$$

$$R_{CO} = 1.3 \times 10^{11} exp\left(\frac{-62{,}700}{T_g}\right) C_{CO} C_{H_2O}^{0.5} C_{O_2}^{0.5} \quad (9)$$

$$R_{H_2} = 3.9 \times 10^{17} exp\left(\frac{-20{,}500}{T_g}\right) C_{H_2}^{0.85} C_{CH_4}^{0.56} C_{O_2}^{1.42} \quad (10)$$

4. Char Burnout

$$C + \alpha O_2 \rightarrow 2(1-\alpha)CO + (2\alpha - 1)CO_2 \quad (11)$$

$$\alpha = \frac{CO}{CO_2} = 2500 exp\left(\frac{-6420}{T}\right) \quad (12)$$

For temperatures between 730 and 1170 K

$$K_d = \frac{5.06 \times 10^{-7}}{d_p} \times \left(\frac{T_s + T_g}{2}\right)^{0.75} \quad (13)$$

$$R_c = \frac{P_{O_2}}{\frac{1}{K_r} + \frac{1}{K_d}} \quad (14)$$

$$K_r = A_c T_s exp\left[\frac{E_c}{RT_s}\right] \quad (15)$$

A_c = 3 kg/m² s kPa and E_c/R = 10300 K

5. NO_x Formation and Reduction in the Bed

By assuming the volatile nitrogen contained in the form of HCN precipitates release rate which is proportional to the rate of release of volatiles, The rate of HCN formation from devolatilized nitrogen is calculated by ω_1:

$$\omega_1 = Y_{Nvol} r_{vol} / M_N \quad (16)$$

where, Y_{Nvol} is the concentration of waste nitrogen volatile, r_{vol} for waste incineration process volatile precipitation rate, M_N atomic weight of nitrogen.

The overall reaction rates of the major nitrogenous species proposed by [23] are

$$\omega_2 = A_1 \times X_{HCN} \times X_{O_2}^b \times exp(-E_1/RT) \quad (17)$$

$$\omega_3 = A_2 \times X_{HCN} \times X_{NO} \times exp(-E_2/RT) \quad (18)$$

$$b = \begin{cases} 0 & X_{O_2} \geq 0.03 \\ -0.35 - 0.1 \times 1gX_{O_2} & 0.03 > X_{O_2} \geq 0.0111 \\ -3.95 - 0.9 \times 1gX_{O_2} & 0.0111 > X_{O_2} \geq 0.0041 \end{cases}$$

where: A_1, A_2 for the reaction constant, E_1, E_2 is the activation energy of the reaction, the values of these constant taken from [24], X_{HCN}, X_{O2} mole concentration of HCN and O_2, respectively, and b is the model coefficients, related to the size and value of the concentration of oxygen related to reaction atmosphere.

For char nitrogen, assuming that directly generate NO, or is reduced to N_2, NO char nitrogen generation reaction rate is:

$$\omega_4 = Y_{Nchar} r_{char} / M_N \quad (19)$$

The heterogeneous NO reduction rate as described by [25] is:

$$\omega_5 = A_3 \times exp(-E_3/RT) \times A_E \times P_{NO} \times \gamma \quad (20)$$

A_E is the specific surface area of char in m^2/kg, P_{NO} for the partial pressure of the gas phase NO in atmospheric pressure, and γ is the changes in the surface area of the reaction of char correlation coefficient due to swelling and fracturing during the reaction process.

B. Transport Equations for Gas and Solid Phases

1. Continuity Equation

Gas Phase:

$$\frac{\partial(\phi\rho_g)}{\partial t} + \nabla(\phi\rho_g u_g) = S_{sg} \quad (21)$$

Solid Phase:

$$\frac{\partial((1-\phi)\rho_s)}{\partial t} + \nabla((1-\phi)\rho_s u_s) = -S_{sg} \quad (22)$$

ϕ is the void fraction in the bed:

$$\phi = \phi^\circ \frac{V_\circ}{V} \quad (23)$$

$$\frac{V_\circ}{V} = 1 - a_1(R^\circ_{dry} - R_{dry}) - a_2(R^\circ_v - R_v) - a_3(R^\circ_c - R_c) \quad (24)$$

V_0 is the initial volume, V is the volume of the particle, a_1, a_2, a_3 are coefficients equal to 1 or 0 according to the appearance of moisture, devolatilization, and char burnout respectively.

S_{sg} is the conversion rate from solid to gases due to evaporation, devolatilization and char burning S_{sg} is the conversion rate from solid to gases due to evaporation, devolatilization and char burning

$$S_{sg} = R_{evp} + R_v + R_c \quad (25)$$

2. Continuity Equation

Gas Phase:

$$\frac{\partial(\phi\rho_g u_g)}{\partial t} + \nabla(\phi\rho_g u_g u_g) = -\phi\nabla P_g + \phi\rho_g g - \beta(u_g - u_s) + \nabla\phi\tau_g \quad (26)$$

The gas–solid inter-phase drag coefficient, β, is calculated as [26], [27]:

$$\beta = 150\frac{(1-\phi)^2\mu_T}{\phi d_p^2} + 1.75\frac{\rho_g(1-\phi)|U_g - U_s|}{d_p} \quad (27)$$

The gas phase stress tensor determined as:

$$\tau_g = \mu_g[\nabla u_g + \nabla u_g^T] - \frac{2}{3}\mu_T(\nabla u_g) \quad (28)$$

$$\mu_T = \mu_g + \mu_t \quad (29)$$

$$\mu_t = \rho_g C_\mu \frac{k^2}{\varepsilon} \quad (30)$$

C_μ is the constant, set as 0.09.

The governing transport equations for k and ε respectively are:

$$\frac{\partial}{\partial t}(\phi\rho_g k) + \nabla(\phi\rho_g u_g k) = +\nabla\left(\phi\frac{\mu_t}{\sigma_k}\nabla k\right) + \phi G_k - \phi\rho_g\epsilon \quad (31)$$

$$\frac{\partial}{\partial t}(\phi\rho_g\varepsilon) + \nabla(\phi\rho_g u_g\varepsilon) + \nabla\left(\phi\frac{\mu_t}{\sigma_\varepsilon}\nabla\varepsilon\right) + \phi(C_{\varepsilon1}G_k - C_{\varepsilon2}\rho_g\epsilon) \quad (32)$$

where G_k represents the generation of turbulence kinetic energy due to the mean velocity gradients and is expressed as:

$$G_k = \mu_t\nabla u_g.[\nabla u_g + \nabla u_g^T] - \frac{2}{3}\nabla u_g(\mu_t\nabla u_g + \rho_g k) \quad (33)$$

$C_{\varepsilon1}$= 1.44 and $C_{\varepsilon2}$ = 1.92, the turbulent Prandtl numbers for k and ε are σ_k = 1 and σ_k = 1.3, respectively [28].

Solid Phase:

$$\frac{\partial((1-\phi)\rho_s u_s)}{\partial t} + \nabla((1-\phi)\rho_s u_s u_s) = -(1-\phi)\nabla P_s + (1-\phi)\rho_s g - \beta(u_g - u_s) + \nabla(1-\phi)\tau_s \quad (34)$$

where the stress tensor of the solid phase (τ_s) and the bulk viscosity (μ_b) is expressed as follows:

$$\tau_s = \left(\mu_b - \frac{2}{3}\mu_s\right)\nabla u_s + \mu_s(\nabla u_s + u_s^T) \quad (35)$$

$$\mu_b = \frac{4}{3}(1-\phi)\rho_s d_p g_o \quad (36)$$

Gidaspow, 1994 [29] described the equation of the solid shear viscosity,μ_s, as:

$$\mu_s = \frac{4}{5}(1-\phi)\rho_s d_p g_o(1+e)\sqrt{\frac{\Theta_s}{\pi}} + \frac{10\rho_s d_p\sqrt{\pi\Theta_s}}{96(1+e)\epsilon g_o}\left[1 + \frac{4}{5}g_o(1-\phi)(1+e)\right]^2 \quad (37)$$

The solid pressure P_s is:

$$P_s = (1-\phi)\rho_s\Theta_s + 2(1+e)(1-\phi)^2 g_o\rho_s\Theta_s \quad (38)$$

For the radial distribution function of solid phase, g_o is expressed as [30], [31]:

$$g_o = \frac{3}{5}\left[1 - \left(\frac{(1-\phi)}{(1-\phi)_{max}}\right)^{\frac{1}{3}}\right]^{-1} \quad (39)$$

The granular temperature Θ_s is a pseudo-temperature, which can be defined as:

$$\frac{3}{2}\Theta_s = \frac{1}{2}\langle u_s' u_s'\rangle \quad (40)$$

The u_s' is the fluctuating velocity of the particles and can be determined by turbulence kinetic energy as:

$$u_s' = \zeta\left(2k/3\right)^{0.5},$$

where ζ is a random number that obeys the Gauss distribution, $0 \leq \zeta \geq 1$.

3. Energy Equation

Gas Phase:

$$\frac{\partial((1-\phi)\rho_s c_{ps} T_s)}{\partial t} + \nabla\left(\phi\rho_g u_g c_{pg} T_g\right) = \nabla\left(\lambda_g . \nabla T_g\right) + A_s h_s'\left(T_g - T_s\right) + S_{T_g} \quad (41)$$

Solid Phase:

$$\frac{\partial\left((1-\phi)\rho_s c_{ps} T_s\right)}{\partial t} + \nabla\left((1-\phi)\rho_s u_s c_{ps} T_s\right) = \nabla\left(k_{eff} . \nabla T_s\right) + (\nabla q_r) - A_s h_s'\left(T_g - T_s\right) + S_{T_s} \quad (42)$$

Rosseland, 1936 [32] gives the radiative flux density as:

$$\nabla q_r = -\frac{16\sigma T^2}{K}(\nabla T)^2 + \frac{16\sigma T^3}{3K}(\nabla^2 T) \quad (43)$$

The thermal dispersion coefficient λ_g can be expressed as:

$$\lambda_g = k_{eff,0} + 0.5 \times d_p \times U_g \times \rho_g \times C_{pg} \quad (44)$$

$$k_{eff,0} = \phi\left(k_f + h_{rv}\Delta l\right) + \frac{(1-\phi)\Delta l}{1/(\frac{k_f}{l_v} + h_{rs}) + l_s/k_s} \quad (45)$$

where $l_s = \frac{2d_p}{3}$, k_s is the thermal conductivity of the pure solid,l_v,h_{rv},h_{rs}, and $\Delta l$are written as:

$$l_v = 0.151912\Delta l\left(\frac{k_f}{k_{air}}\right) \quad (46)$$

$$h_{rv} = 0.1952\left(1 + \frac{\phi(1-\epsilon)}{2(1-\phi)\epsilon}\right)^{-1}\left(\frac{T_s}{100}\right)^n \quad (47)$$

$$h_{rs} = 0.1952 \times d_p\left(\frac{\epsilon}{2-\epsilon}\right)\left(\frac{T_s}{100}\right)^n \quad (48)$$

$$\Delta l = 0.96795\, d_p(1-\phi)^{-1/3} \quad (49)$$

k_{air} is the air thermal conductivity,

$$k_{air}(T_g) = 5.66 \times 10^{-5} T_g + 1.1 \times 10^{-2} \quad (50)$$

(n) is an empirical parameter related to the fuel packing conditions. In this model,

$$n = 1.93 + 0.67\exp\left(-\frac{(m_g - 0.39)}{0.054}\right) \quad (51)$$

Source term of the energy equation for both gas and solid is calculated as:

$$S_{Tg} = -R_{evp} \times h_{f,CO} \quad (52)$$

$$S_{Ts} = -R_{evp} \times \frac{M_{CO}}{M_c} \times \left[h_{f,CO2} - h_{f,CO}\right] \times \left[\frac{Y_{CO}}{2} - 1\right] \quad (53)$$

4. Species Equation

Gas Phase:

$$\frac{\partial\left(\phi\rho_g Y_{ig}\right)}{\partial t} + \nabla\left(\phi\rho_g u_g Y_{ig}\right) = \nabla\left(D_{ig}\nabla\left(\phi\rho_g Y_{ig}\right)\right) + S_{Y_g} \quad (54)$$

Solid Phase:

$$\frac{\partial((1-\phi)\rho_s Y_{is})}{\partial t} + \nabla((1-\phi)\rho_s u_s Y_{is}) = S_{Y_s} \quad (55)$$

IV. Numerical Method and Boundary Conditions

The whole geometrical domain of the bed is divided into a number of small cells, which is discretized over each cell and solved numerically using the SIMPLE algorithm [33], [34]. The computational grid was adapted in each time step to the height of the bed. The staggered grid was utilized, which set vectors at the boundaries of cells and scalars at the center. The partial differential equations were discretized by the finite volume method (FVM) using the Upwind Difference Scheme.

The used material sample weight is 2kg, and its main components are analyzed in Tables I and II. The average height of the bed is 530mm, and bulk density of original material is 148.29 kg/m^3, while the void ratio is 0.6. This experiment was carried out below room temperature, as the primary air temperature was 20°C, using a different primary air quantity entering from the grate to the bed layers; parameters of primary air flow are shown in Table III.

TABLE I
PROPORTION OF SIMULATED MSW

MSW sample	Cardboard	Vegetables	Ash
Proportion	50	30	20

TABLE II
ANALYSIS OF SIMULATED MSW

Proximate analysis	Moisture	Volatile	Fixed carbon	Ash	Low calorific value
%	26.5	38.25	4.55	30.7	6.56
Ultimate analysis	C	H	O	N	S
%	19.81	2.47	20.37	0.06	0.09

TABLE III
PRIMARY AIR FLOW RATES OF TESTS (PRIMARY AIR TEMPERATURE: 20℃)

case	1	2	3	4	5	6	7
flow rate (L/min)	25	33	70	95	105	160	200

V. Results and Discussion

According to the simulation results, the temperature distribution contour is shown in Fig. 2. It is shown that MSW incineration process undergoes four stages: moisture evaporation, pyrolysis, combustion, and after-combustion. The first stage is drying, where moisture in waste material will be vaporized entirely when reaching 100°C or above. Moisture evaporation in waste takes a long time, taking up most of the time needed for material incineration, so it is the main principle that determines the time taken for incineration. When the evaporation temperature of moisture in material gets closer

to 100°C, material combustion fronts absorb a lot of heat, and that is the reason why moisture amount decreases. The next processes are pyrolysis and ignition. Pyrolysis temperature is usually 260°C [23]. When the temperature of material gets close to 260°C, the distance between pyrolysis starting temperature curve and evaporation curve is very slight, and in this area material drying temperature increases very rapidly.

When starting temperature curve of pyrolysis is formed, temperature gradient increases, this is mainly because large amount of heat devolatilize, and rapidly ignites and burns, making combustion fronts propagate downwards (temperature of 300°C is considered the time when volatile components in simulated waste start to burn). Flame fronts are formed after ignition, fixed bed height points move together towards the fire grate according to the flame fronts. There are two distinct high-temperature areas near the surface of the fixed bed; the first is caused by the common function of both the upper layer and hot gas combustion radiation; the second appears when the height of the bed is approximately 200mm, mainly because after the material ignites and burns, by the end of combustion a large amount of unburned coke accumulates, also oxygen concentration near fire grates increases, air disturbance becomes greater, coke and air mix better, and coke burns rapidly forming high temperature area. This is similar to the results of the simulations held by [35] and [8].

As primary air flow increases, the height of high temperature areas also increases, but after reaching a specific extent no further changes may occur; the highest reaction temperature increases first then decreases, as shown in Fig. 5. This is mainly determined by the heat transfer nature of both gas and solid in the fixed bed. When the primary air flow increases, bed material cooling speed increases, and after reaching a certain value, the bed temperature may decrease. The numerical simulation and analysis were made, and good agreement was indicated between the current model and the experimental work.

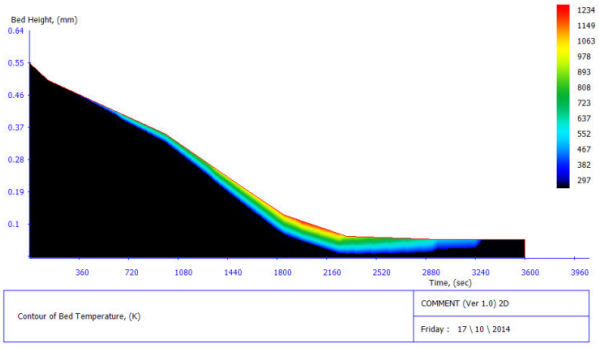

Fig. 2 Contour of temperature (K) inside the fuel bed versus time (flow rate: 95L/min)

It is shown in Fig. 4 that during stable combustion, the speed of flame propagation is fixed, and speed of material combustion is constant, also propagation speed of flame fronts is conserved, and this is due to the conservation of moisture evaporation speed in the combustion process and lightness of combustion fronts; with the increase of the primary air flow rate, flame propagation speed increases firstly, then decreases till it reaches a certain extent then it keeps constant, which is a conclusion is similar to that of [36]. When the primary air flow rate reaches a certain value it continues to increase afterwards, excess primary air (cool air) decreases the temperature of ignition fronts and combustion chamber.

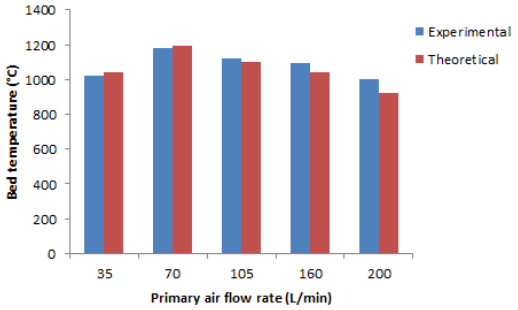

Fig. 3 Comparison between experimental and theoretical results of bed maximum temperature (K) with different primary air flow rate

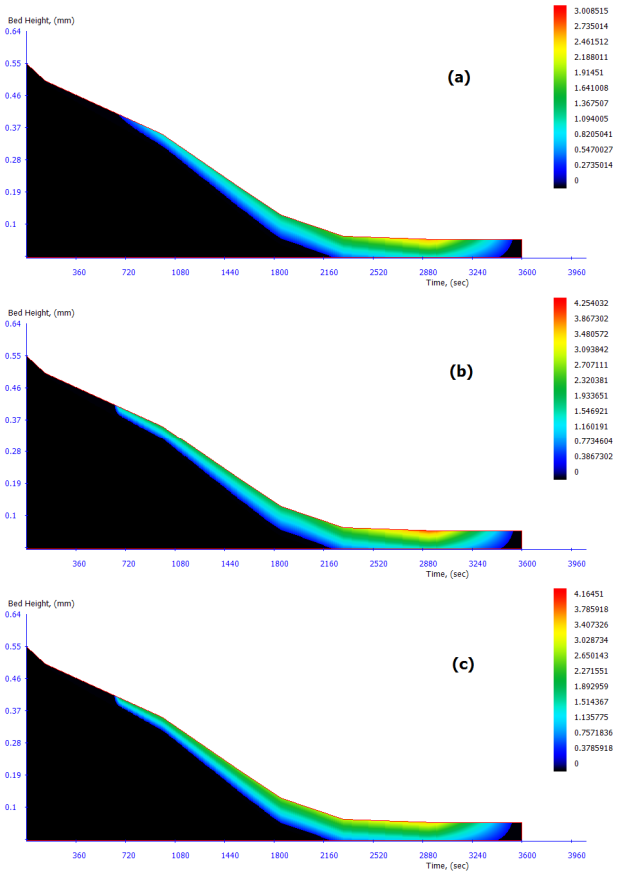

Fig. 4 Contour of velocity of flame ignition front (m/s) in bed at different primary air flow rate; (a) 35 L/min, (b) 70 L/min, (c) 105 L/min

It is shown in Fig. 5 that at the beginning CH_4 concentration in measuring point 1 is higher than in measuring points 2 and

3, this is mainly because flame fronts propagate from the top layers of the fixed bed to the bottom layers; thus materials at the top of the fixed bed start to burn, leading to a large amount of devolatization, then after a certain time combustion fronts start to propagate downwards.

When t = 1860s, CH_4 concentration in measuring point 1 is lower than in point 2, this is mainly because CH_4 continues to burn when flue gas increases, causing CH_4 concentration in measuring point 1 to decrease. Whilst at t = 2900s, devolatization is completed. When t=3000s, char combustion is completed, thus the whole combustion process is completed, and temperature in measuring points decreases rapidly.

However, when the primary air flow rate is low, material combustion speed is low too, at this moment N and the oxygen reaction speed decreases accordingly, and oxygen concentration around material decreases; thus, NO concentration is low too, reactions at this moment are mainly restricted by oxygen concentration, causing N/ NO conversion rate to decrease. As the primary air flow rate increases, combustion speed of material increases, and NO concentration increases significantly for a certain period.

The conversion ratio also has been compared in the present study experimentally and theoretically as shown in Fig. 6. The comparison is very proficient and the consequences of the present model having the same approximately values.

After primary air flow rate reaches a certain extent and starts to increase, carbon content in ash residue is increased, and incomplete combustion resulted, this is mainly because of the following; as primary air flow rate increases, primary air cooling effect on the lower layers of material increases and reaction speed is decreased. When primary air flow rate decreases, combustion speed decreases, and ash residue also contain a large amount of unburned carbon. The good agreement between the experimental and the present model can be observed from Fig. 7.

The experiment is also carried out in the bottom area for the different primary air temperature when the air flow rate reaches 35L/min (20, 60 and 80°C) and 130L/min (20, 50, 70 and 100°C), to investigate the effect of primary air temperature on the combustion process for MSW.

The simulation results show that as primary air temperature increases, temperature in high temperature areas increases very slightly. It is shown in Fig. 8 that there are slight changes in areas of high temperature regions. Primary air supplied to the bottom of the combustion chamber heats up the material at the bottom areas, causing the moisture content in these materials to decrease.

When these materials reach combustion temperature, heat absorbed is decreased, also these materials release a large amount of heat; as a result, and there is a slight increase in the temperature of high temperature areas.

It is shown in Fig. 9 that as the primary air temperature increases, CO average emission concentration increases gradually. This is mainly because propagation of combustion in the fixed bed is increased, also combustion reactions are vigorous, and release of volatile component separation is increased, causing the concentration of CO to increase in a very short time. Fig. 9 also proves that NO highest concentration peak is slightly affected by primary air temperature.

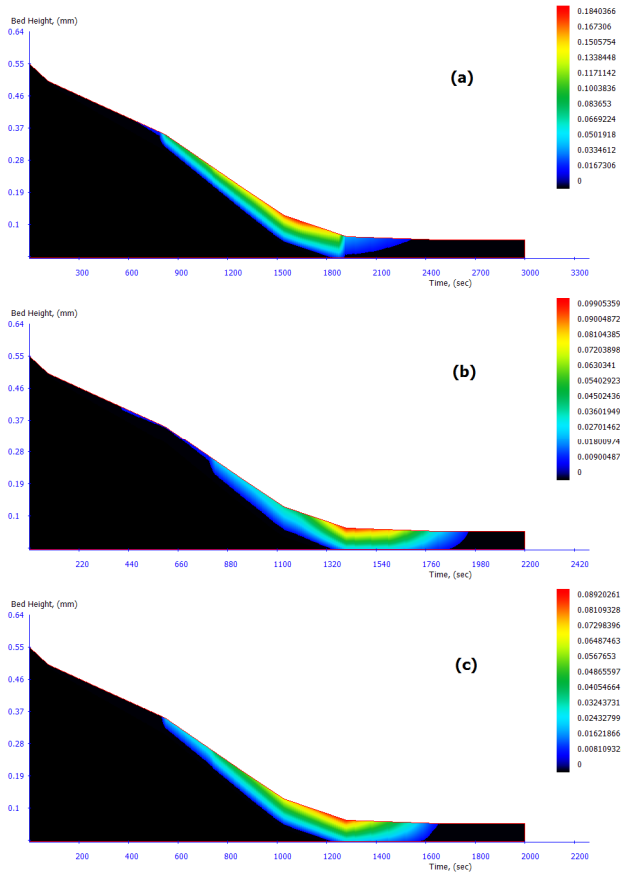

Fig. 5 Contour of CH_4 with time at different primary air flow rate (1 Sampling position); (a) 35 L/min, (b) 70 L/min, (c) 105 L/min

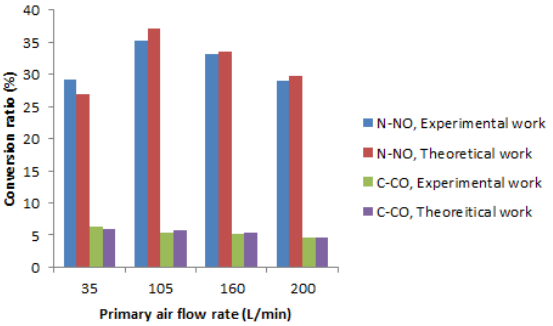

Fig. 6 Comparison between experimental and theoretical results of conversion ratio (%) of N to NO and C to CO with different primary air

This is because char combustion propagate in the latest stage is close to combustion of volatile, thus their peaks are very close. It is shown in Fig. 10 that as the primary air temperature increases, NO average emission concentration increases gradually.

This is mainly because when the primary air temperature increases, material combustion speed also increases, and during combustion average temperature is higher and devolatization is faster, also carbon reaction speed increases; therefore, NO average emission concentration increases gradually during the whole process of material combustion.

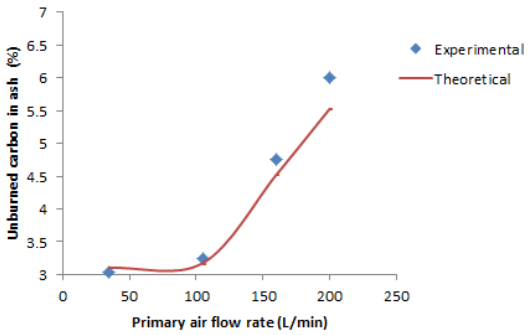

Fig. 7 Unburned carbon in ash with different primary air flow rate, experimentally and numerically.

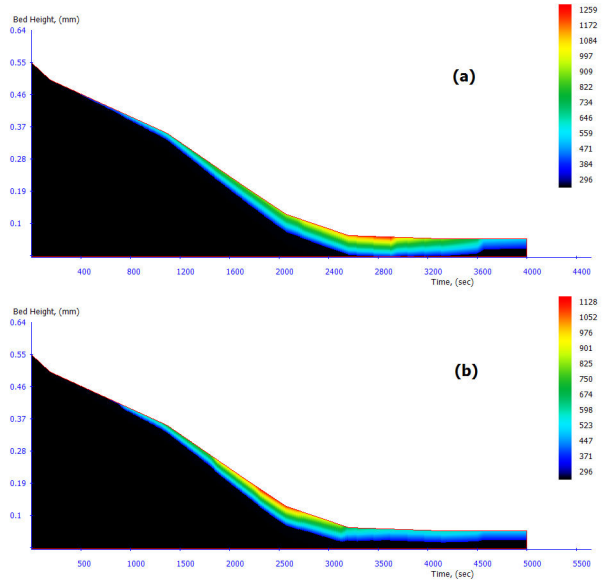

Fig. 8 Contour of temperature (K) inside the fuel bed versus time; (a) primary air temperature primary air 60°C, (b) primary air temperature 80°C, at flow rate: 35L/min

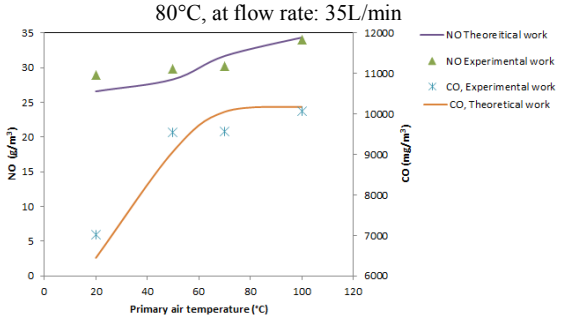

Fig. 9 Average emission concentration of NO and CO with different primary air temperature; flow rate: 130L/min

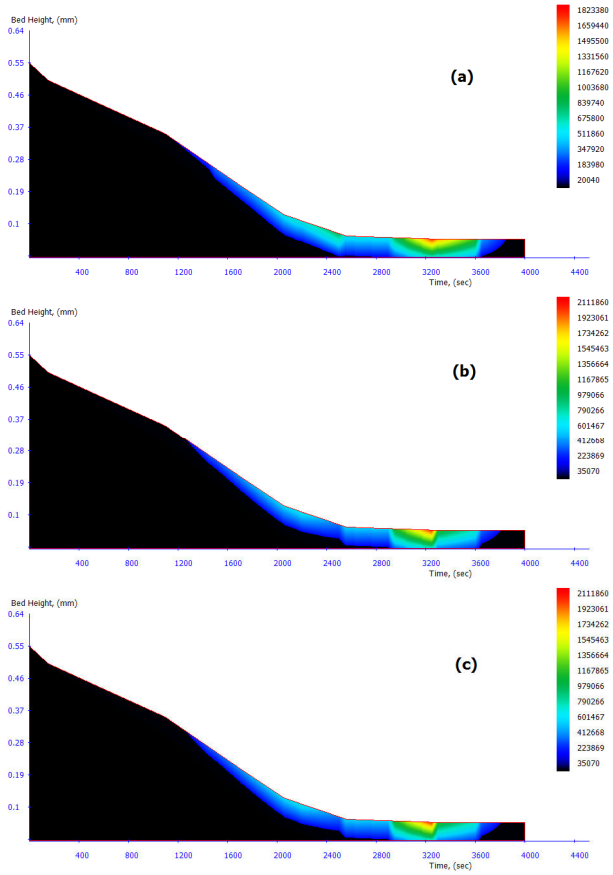

Fig. 10 Contour of NO concentration (% vol) with time at different primary air temperature; (a) 20°C, (b) 50°C, (c) 70°C, flow rate 130 L/min

It is shown in Fig. 11 that when the primary air temperature increases, there appears to be no any significant changes in CH_4 highest concentration peak, which proves that CH_4 highest concentration peak is slightly affected by primary air temperature. This is because the char combustion speed in the latest stage is close to volatile release, thus their peaks are very close. As primary air temperature increases, there is a very slight increase in char burning; the concurrence between the experimental and the present model can be shown from Fig. 12.

VI. Conclusion

The simulation results are compared with experimental data, which shows that the incineration process of waste in the fixed bed is reasonably simulated.

Eulerian-Eulerian CFD model incorporating the kinetic theory of granular flow was applied, by developing a novel mathematical model in the form of COMMENT code applicable for predicting combustion process of solid fuel under different parameters, giving a promise way in its capability and sensitivity for the parameter effects that influence the incineration process. The model provides information concerning temperature, front propagation,

reaction front rate, as well as remaining gas species composition in bed.

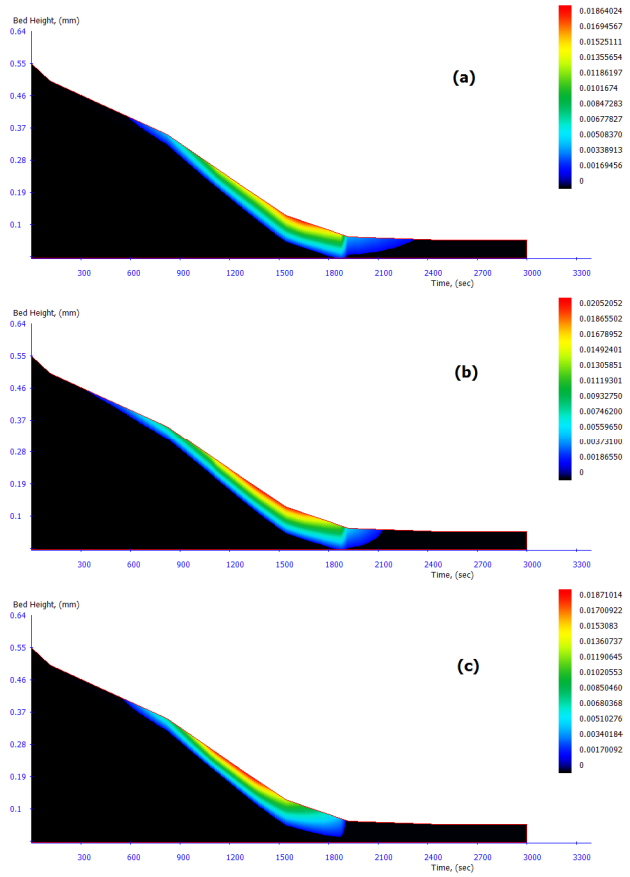

Fig. 11 Contour of CH_4 concentration (% vol) with time at different primary air temperature; (a) 20°C, (b) 60°C, (c) 80°C, at flow rate: 30 L/min, (1 Sampling position, 1—388mm)

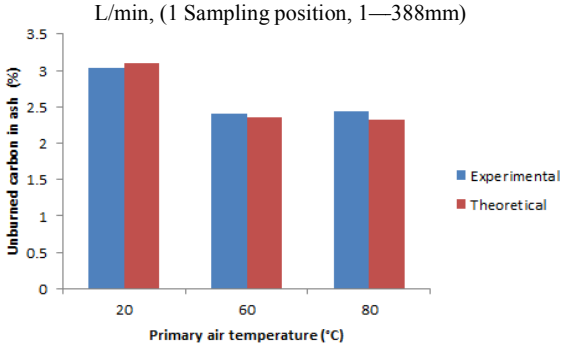

Fig. 12 Unburned carbon in ash with different primary air temperature, experimentally and numerically, at flow rate: 30L/min

It is found that the average concentration of CO and the conversion ratio of C to CO are inversely proportional to primary air flow rate; the conversion ratio of N to NO rises as the primary air flow increases and reaches a peak point at the critical air flow rate, after that the conversion ratio of N to NO declines as the air flow further increases; with the increase of primary air temperature, the average concentration of CO and NO, but the highest concentration of NO changes hardly.

When the primary air temperature is lower than 100°C, the average flame front increases only a little, but the flame front increases faster near the grate; the total mass loss rate and moisture evaporation rate increase only a little with the increase of primary air temperature; with the increase of moisture and ash content, the flame propagation speed and the burning rate decrease.

NOMENCLATURE

A	pre-exponent factor, particle surface area 1/s, m²
C_p	specific heat capacity J/kg K
C_{mix}	mixing rate constant
$C_{w,g}$	moisture concentration in the gas phase kg/m³
$C_{w,s}$	moisture concentration at the solid phase kg/m³
D_g	mass diffusion coefficient of gas m²/s
D_{O2}	mass diffusion coefficient of oxygen m²/s
d_p	particle diameter m
E	activation energy kJ/mol
e	coefficient of restitution for particle collisions
g_o	radial distribution function
H_{evp}	evaporation heat of the solid material J/kg
h_f	enthalpy of formation J/kg
h_{rs}	radiation heat transfer coefficient m/s
h_{rv}	effective radiation heat transfer coefficient of the voids m/s
h_s	convective mass transfer coefficient
$h_{s'}$	convection heat transfer coefficient W/m² K
I	radiative intensity W
K	extinction coefficient
K	turbulent kinetic energy m²/s²
k_d	diffusion rates kg/atm m² s
k_f	thermal conductivity of the fluid W/mK
k_s	thermal conductivity of the pure W/mK
k_{eff}	effective thermal conductivity W/mK
$k_{eff,0}$	thermal conductivity for no fluid flow W/mK
l_s	equivalent thickness a layer of solid m
M	molecular weight kg/kmol
Q_{cr}	heat absorbed by the solid W
q_r	radiative flux density W
R	gas universal constant J/kmol K
R_{evp}	moisture evaporation rate kg/s
R_c	char consumption rate kg/s
Rv	volatile matter in solid rate kg/s
R_{wg}	water gas shift reaction kg/s
S_Φ	Source term
T_{env}	environment temperature K
T_g	gas temperature K
T_s	solid temperature K
X	species generation
Y_v	mass fraction of volatile matter
U	velocity component m/s
Greek Letters	
α	absorption coefficient
B	drag coefficient
μ	dynamic viscosity kg/m s
Φ	void fraction in bed
ε	dissipation rate of turbulent kinetic energy $m^{-2}s^{-3}$
ϵ	Emissivity
σ_p	scattering coefficient
δ	Stephane-Boltzmann constant W/m² K^4
ρ	density kg/m³

λ_g thermal dispersion coefficient
λ_{mix} effective dispersion coefficient
Φ dependent variable
τ_s stress tensor Pa

Subscripts

b Bulk
C char burnout
eff Effective
f Fluid
g Gas
p Particle
s Solid
sg solid to gas

REFERENCES

[1] Ligang Liang, Rui Sun, Qiang Guo, Kui Dai, Shaohua Wu. Experimental Study on Combustion of Simulated Municipal Solid Wastes in a Fixed Bed. 4th i-CIPEC, September 26-29, 2006, Kyoto, Japan.
[2] H. Thunman, L-E. Amand, F. Ghirelli, et al. Modelling and verifying experiments on the whole furnace principles and models of solid fuel combustion. Chalmers University of Technology, 2001.
[3] M.J.V. Goldschmidt, R. Beetstra, J.A.M. Kuipers, Hydrodynamic modeling of dense gas-fluidized beds: comparison of the kinetic theory of granular flow with 3D hard-sphere discrete particle simulations, Chemical Engineering Science, 57 (2002), 2059–2075.
[4] S. Benyahia, H. Arastoopour, T.M. Knowlton, H. Massah, Simulation of particles and gas flow behavior in the riser section of a circulating fluidized bed using the kinetic theory approach for the particulate phase, Powder Technology 112 (2000), 24–33.
[5] P.T. Radulovic, M.U. Ghani, L.D. Smoot, An improved model for fixed bed coal combustion and gasification, Fuel 74 (1995), 582–594.
[6] Y. B. Yang, V. N. Sharifi, J. Swithenbank. Effect of air flow rate and fuel moisture on the burning behaviours of biomass and simulated municipal solid wastes in packed beds. Fuel, 2004, 83(11-12): 1553-1562
[7] Y. B. Yang, H. Yamauchi, V. Nasserzadeh, et al. Effects of fuel devolatilization on the combustion of wood chips and incineration of simulated municipal solid wastes in a packed bed. Fuel, 2003, 82(18): 2205-2221
[8] C. Ryu, D. Shin, S. Choi. Effect of fuel layer mixing in the waste bed combustion. Advances in Environmental Research, 2001, 5(3): 259-267
[9] J. J. Saastanainen, R. Taipale, M. Horttanainen, et al. Propagation of the ignition front in beds of wood particles. Combustion and Flame, 2000, 123(1-2): 214-226
[10] Y. R. Goh, R. G. Siddall, V. Nasserzadeh, et al. Mathematical modeling of the waste incinerator burning bed. J Inst Energy, 1998, 71: 110-118
[11] Y. R .Goh, C. N. Lim, K.H. Chan, et al. Mixing, modelling and measurements of incinerator bed combustion. The Second International Symposium on Incineration and Flue Gas Treatment Technology, 1999: 4-6
[12] R. Zakaria, Y. R. Goh, Y. B. Yang, et al. Reduction of NOx emission from the burning bed in a municipal solid waste incinerator. The Fifth European Conference on Industrial Furnaces and Boilers, Espinho-Porto-Portugal, 2000: 11-14
[13] M. Rönnbäck, M. Axell, L. Gustavsson. Combustion processes in a biomass fuel bed–experimental results. Progress in Thermochemical Conversion, Tyrol, Austria, 2000, 17-22
[14] V. N. Sharifi. Optimization study of incineration in a MSW incinerator with a vertical radiation Shaft. PhD Thesis. 1990
[15] Y. Tsuji, Activities in discrete particle simulation in Japan, Powder Technology 113 (2000), 278–286.
[16] P.D. Cudall, O.D.L.A. Strack, Discrete numerical model for granular assemblies, Geotechnique 29 (1979), 47–65.
[17] J. Ding, D. Gidaspow, A bubbling fluidization model using kinetic theory of granular flow, AIChE Journal 36 (1990), 523–538.
[18] D. Gidaspow, Multiphase Flow and Fluidization: Continuum and Kinetic Theory Description, Academic Press, San Diego, 1994.
[19] Rui Sun, Tamer M. Ismail, Xiaohan Ren, M. Abd El-Salam. Numerical and Experimental Studies on Effects of Moisture Content on Combustion Characteristics of Simulated Municipal Solid Wastes in a Fixed Bed. Waste Management in Press, Corrected Proof, Available online 4 March 2015.
[20] T.M. Ismail, M. Abd El-Salam, M.A. El-Kady, S.M. El-Haggar, Three dimensional model of transport and chemical late phenomena on a MSW incinerator, International Journal of Thermal Sciences 77 (2014), 139-157.
[21] Ligang Liang, Rui Sun, Jun Fei, Shaohua Wu, Xiang Liu, Kui Dai, Na Yao, Experimental study on effects of moisture content on combustion characteristics of simulated municipal solid wastes in a fixed bed, Bioresource Technology 99 (2008) 7238–7246.
[22] B. Peters, N. Thomas, B. Christian, 2003. Modeling wood combustion under fixed bed conditions. Fuel, 82, 729–738.
[23] De Soete, G.G., 1975. Overall reaction rates of NO and N2 formation from fuel nitrogen. In: Fifteenth Symposium (International) on Combustion. The Combustion Institute, Pittsburgh, PA, pp. 1093–1102.
[24] S. C. Hill, L. D. Smoot., 2000. Modeling of nitrogen oxides formation and destruction in combustion systems. Progress in Energy and Combustion Science 26(4): 417-458.
[25] Levy JM, Chen LK, Sarofim AF, Baer JM. Eighteenth Symposium (International) on Combustion, the Combustion Institute, Pittsburgh, PA, 1981. p. 111.
[26] Di Blasi C, 2004. Modeling wood gasification in a countercurrent fixed-bed reactor, AIChE Journal, 50, 9.
[27] J. Cooper, W. L. H. Hallett, 2000. A Numerical Model for Packed-Bed Combustion of Char Particles. Chemical Engineering Science, 55, 4451–4460.
[28] Launder, b. E. and Spalding, D. B. The numerical computations of turbulent flows. 1974.
[29] D. Gidaspow, 1994. A Bubbling Fluidization Model Using Kinetic Theory of Granular Flow. AIChE Journal, 32, 1, 523–538.
[30] S. Hermann, 1979. Boundary layer theory. McGraw-Hill, Seventh Edition.
[31] H. Arastoopour, 2001. Numerical simulation and experimental analysis of gas-solid flow systems: 1999 fluor-daniel plenary lecture, Powder Technology, 119, 59-67.
[32] Rosseland, S., Theoretical Astrophysics: Atomic Theory and the Analysis of Stellar Atmospheres and Envelopes, Oxford, UK: Clarendon, 1936.
[33] S.V. Patankar, Numerical Heat Transfer and Fluid Flow, Hemisphere, 1980.
[34] W.Q. Tao, Numerical Heat Transfer, second ed., Xi'an Jiaotong University, Xi'an, 2001.
[35] D. Shin, S. Choi. The combustion of simulated waste particles in a fixed bed. Combustion and Flame, 2000, 121 (1-2): 167-180.
[36] Zhou, H., Jensen, A.D., Glarborg, P., et al., 2005. Numerical modeling of straw combustion in a fixed bed. Fuel 84 (4), 389–403.